Low-Temperature (450 °C) Crystallization of Al:HfO_2 Ferroelectric Thin Films Enabled by Microwave Annealing Process

Giuk Kim, Lingwei Zhang, Sangho Lee, *Graduate Student Member, IEEE*, Hunbeom Shin, Youngjin Lim, Kang Kim, *Graduate Student Member, IEEE*, Il-Kwon Oh, Sang-Hee Ko Park, Jinho Ahn, and Sanghun Jeon, *Senior Member, IEEE*

***Abstract*— The crystallization of HAO ferroelectric (FE) material requires high annealing temperatures ranging from 700 °C to 1000 °C, because of the smaller ionic radius of Al dopants. This extreme temperature requirement poses substantial challenges for the broad application of the HAO FE layer. Herein, we address this problem by introducing the microwave annealing (MWA) system, capable of inducing the phase transformation essential for FE material crystallization efficiently through a synergistic application of heat and microwaves. The MWA system supplies the activation energy required for the crystallization of hafnia FE materials via a combination of thermal and microwave energy. This allows for a significant reduction in the annealing temperature. Ultimately, we successfully achieved high-quality orthorhombic (o-) phase ($2P_r$ of 24.63 $\mu C/cm^2$) crystallization of HAO at a notably lower temperature of 450 °C. The MWA system-based low-temperature crystallization process significantly improves the interface quality, yielding better results than typical rapid thermal annealing (RTA) at 700 °C. These advancements not only enhance reliability but also diminish the leakage current of HAO. This research is noteworthy as it demonstrates successful polarization switching in HAO FE material under low thermal budget conditions (≤450 °C) enabled by the MWA system.**

Received 20 May 2025; revised 18 June 2025; accepted 4 August 2025. Date of publication 21 August 2025; date of current version 24 September 2025. This work was supported in part by Samsung Electronics Co., Ltd., under Grant IO241203-11376-01; in part by the Korea Collaborative and High-tech Initiative for Prospective Semiconductor Research (K-CHIPS) under Grant 1415187675, Grant 00235655, Grant 23006-15TC, Grant 1415187390, Grant 00231985, Grant 23005-30FC, Grant 2410000582, Grant 00406007, and Grant 24051-15TC; and in part by the Ministry of Trade, Industry and Energy (MOTIE, Korea) and [Ministry of Science and ICT (MSIT)] in Korea under Grant RS-2023-00260527. The review of this article was arranged by Editor T.-H. Kim. *(Giuk Kim and Lingwei Zhang contributed equally to this work.) (Corresponding authors: Jinho Ahn; Sanghun Jeon.)*

Giuk Kim, Lingwei Zhang, Sangho Lee, Hunbeom Shin, and Sanghun Jeon are with the School of EE, KAIST, Daejeon 34141, South Korea (e-mail: jeonsh@kaist.ac.kr).

Youngjin Lim and Il-Kwon Oh are with the Division of ECE, Ajou University, Suwon 16499, South Korea.

Kang Kim and Sang-Hee Ko Park are with the School of MSE, KAIST, Daejeon 34141, South Korea.

Jinho Ahn is with the Division of MSE, Hanyang University, Seoul 04763, South Korea (e-mail: jhahn@hanyang.ac.kr).

Digital Object Identifier 10.1109/TED.2025.3599825

***Index Terms*— Ferroelectric, HAO, $HfAlO_x$, low-temperature annealing, microwave annealing (MWA).**

I. Introduction

HAFNIA ferroelectric (FE) materials are characterized by a noncentrosymmetric orthorhombic (o-phase) crystal structure, which gives rise to robust polarization properties [1], [2], [3], [4]. These characteristics are essential for the operation of various FE memory devices [5], [6], [7]. In particular, polarization switching behavior enables multilevel operation, facilitating the use of FE materials in both memory and neuromorphic devices [8], [9], [10]. Consequently, extensive research has focused on stabilizing and enhancing the FE o-phase to improve device performance [11], [12], [13].

To this end, hafnia-based FE materials doped with various elements, such as Al, Zr, Sr, Y, and Gd, have been widely investigated [14], [15], [16], [17], [18]. Among them, Al dopants, which possess a smaller ionic radius than Hf, have been reported to increase the energy barrier for the phase transition from tetragonal (t-phase) to monoclinic (m-phase) during annealing, thereby enhancing thermal stability [6]. In addition, $HfAlO_x$ (HAO) has shown a high dielectric response ($\kappa \approx 68$) when a morphotropic phase boundary (MPB) state is achieved through precise compositional and annealing control [19]. These findings suggest that HAO-based FE materials hold great potential for a wide range of applications.

Despite this promise, HAO FE films typically require high-temperature annealing (700 °C–1000 °C), which leads to significant degradation in FE properties [6], [20], [21], [22]. Moreover, such thermal conditions promote the formation of interfacial dead layers, resulting in increased leakage current and severe reliability issues [23], [24], [25], [26]. To address these challenges, a microwave annealing (MWA) system capable of low-temperature processing has been suggested [27]. Unlike typical annealing methods, such as furnace or rapid thermal annealing (RTA), which rely solely on thermal energy, the MWA process delivers energy via both heat and microwave irradiation, enabling effective crystallization of FE films at a significantly reduced thermal budget [28], [29].

1557-9646 © 2025 IEEE. All rights reserved, including rights for text and data mining, and training of artificial intelligence and similar technologies. Personal use is permitted, but republication/redistribution requires IEEE permission.
See https://www.ieee.org/publications/rights/index.html for more information.
Authorized licensed use limited to: Korea Advanced Inst of Science & Tech - KAIST. Downloaded on December 01,2025 at 09:32:13 UTC from IEEE Xplore. Restrictions apply.

Here, we achieved FE o-phase crystallization in HAO films using an MWA system at a record low temperature of 450 °C. While the RTA-annealed sample at 700 °C exhibited a remnant polarization ($2P_r$) value of 16.53 μC/cm^2, the MWA-annealed sample at 450 °C demonstrated an enhanced $2P_r$ of 24.63 μC/cm^2, a 49% improvement. In addition, the leakage current density at 1 V was reduced by 68%, from 3.89×10^{-8} A/cm^2 for the RTA sample to 1.26×10^{-8} A/cm^2 for the MWA sample. These improvements are attributed to the suppression of interfacial dead layer formation, enabled by the lower crystallization temperature of the MWA process. Specifically, MWA process effectively minimizes unwanted interactions between the TiN and HAO, improving interface quality and device reliability. These findings demonstrate the potential of MWA-treated HAO FEs for future applications.

II. Experimental Details

For the metal–$HfAlO_x$ FE–metal (MFM) capacitor, TiN bottom electrodes were deposited onto a Si/SiO_2 substrate via sputtering to a thickness of 100 nm. Subsequently, an Al-doped HfO_2 FE layer was deposited using a plasma-enhanced atomic layer deposition (PEALD) system with an Al doping ratio of 29:1. In this study, the thickness of all HAO films was uniformly maintained at 10 nm. The substrate temperature was maintained at 320 °C. TEMA-Hf and TMA were used as precursors for HfO_2 and AlO, respectively. The top TiN electrodes were then deposited via sputtering to a thickness of 50 nm, followed by standard patterning and wet etching processes. The MWA samples were annealed in an N_2 atmosphere for 10 s under various annealing temperature conditions. Pulse measurements and various electrical measurements were conducted using a Keithley-4200A-SCS (Keithley), pulse generator (81110A, Agilent), and CX-3324A (Keysight) parameter analyzer.

The MWA process enables volumetric heating through dipole rotation and conduction loss, allowing effective energy delivery into the interior of the thin film. This leads to rapid and uniform crystallization even at temperatures below 450 °C. In this study, a customized MWA setup was used. The microwave frequency was set to 2.45 GHz with a maximum output power of 3 kW. To monitor the annealing temperature, a thermocouple is placed in direct contact with the silicon carbide (SiC) susceptor. The samples are annealed on the SiC susceptor under a nitrogen ambient, which are selected to suppress unwanted oxidation and ensure both uniform thermal distribution and efficient microwave absorption in the hafnia-based FE films.

III. Results and Discussion

Fig. 1(a) presents the schematic of the MWA system used in this study. To determine the optimal annealing temperature for the HAO films, MWA process at various temperatures ranging from 400 °C to 600 °C was conducted. The dielectric displacement–electric field (D–E) and corresponding capacitance–voltage (C–V) curves of the woken-up MFM capacitors are shown in Fig. 1(b) and (c). The wake-up process was identically performed on all devices under an electric field of 3.5 MV/cm for 10^4 cycles. Since a portion of the

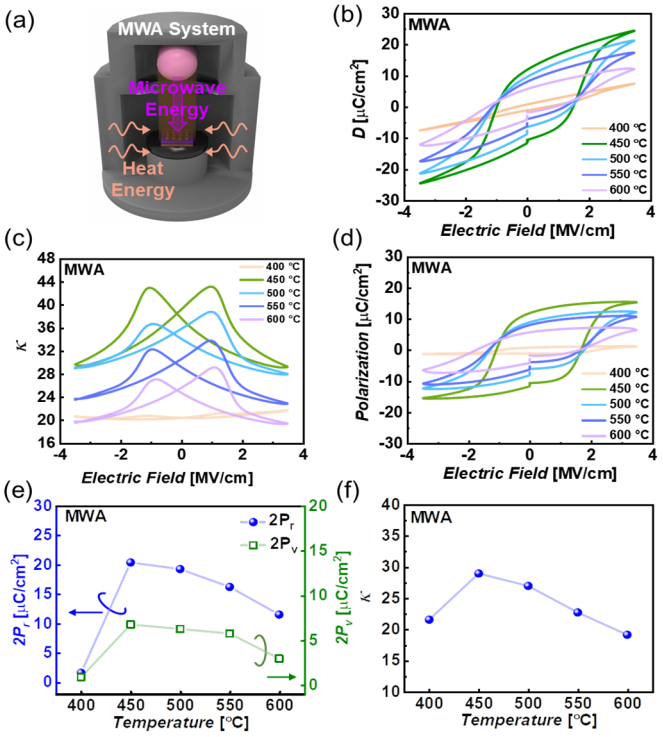

Fig. 1. (a) Schematic of MWA system. Experimental (b) D–E and (c) κ–V curves of FE capacitors with MWA at varying annealing temperatures. Extracted (d) P–E curves, (e) $2P_r$ values, $2P_V$ values, and (f) κ values of MWA samples.

total dielectric displacement originates from the dielectric component, the pure polarization–electric field (P–E) curves were extracted by subtracting the linear dielectric contribution, as shown in Fig. 1(d) [30]. Fig. 1(e) and (f) presents the extracted values of $2P_r$, variable polarization ($2P_V$), and dielectric constant (κ) for the HAO films crystallized via MWA at different temperatures. The P_V value is obtained by subtracting P_r from the saturation polarization (P_S) in the pure P–E curve. The $2P_r$ and $2P_V$ parameters represent the relative amounts of the FE o-phase and the antiferroelectric t-phase, respectively [6]. Moreover, considering that m-phase shows a κ value below 20, the phase distribution within the HAO film under different MWA conditions can be qualitatively and comparatively inferred using these three parameters: $2P_r$, $2P_V$, and κ.

It is generally known that during the annealing process, the t-phase is stabilized within hafnia FE films, while phase transitions to the o-phase and m-phase occur during the cooling process. Under the MWA 400 °C condition, the phase transition from amorphous to crystalline appears to be minimal. In contrast, the high values of $2P_r$, $2P_V$, and κ observed at 450 °C suggest the dominance of the o-phase and t-phase. However, when the annealing temperature exceeds 450 °C, the simultaneous decrease in all three parameters implies that a significant portion of the t-phase transforms into the m-phase during the cooling process [6]. Additionally, the formation of interfacial dead layers further contributes to the reduction in these parameters and polarization performance.

Fig. 2(a)–(d) presents the phase analysis results of samples processed via MWA and RTA systems. The $2P_r$, $2P_V$, and

Authorized licensed use limited to: Korea Advanced Inst of Science & Tech - KAIST. Downloaded on December 01,2025 at 09:32:13 UTC from IEEE Xplore. Restrictions apply.

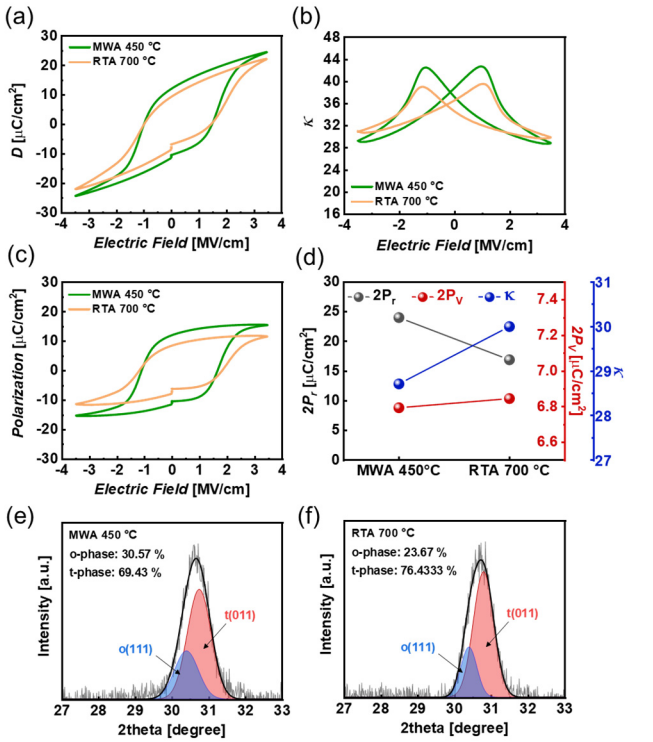

Fig. 2. Comparison of (a) D–E curves, (b) κ–V curves, (c) D–E curves, and (d) $2P_r$, $2P_V$, and κ values resulting from MWA and RTA treatments. GIXRD analysis results of (e) MWA and (f) RTA pristine samples, respectively.

κ values of the HAO films annealed by MWA at 450 °C are comparable to those of the films annealed by RTA at 700 °C. This suggests that MWA at 450 °C induces a similar degree of crystallization in the HAO films as RTA at 700 °C. More specifically, the extracted parameters indicate that MWA-treated HAO film contains a higher fraction of the o-phase and a lower fraction of the t-phase compared to RTA-treated film. This trend is further supported by the grazing incidence X-ray diffraction (GIXRD) analysis, as depicted in Fig. 2(e) and (f), which shows that MWA samples exhibit a higher o-phase content than RTA samples, even under lower annealing conditions. These results suggest that the MWA system can effectively supply the activation energy required for o-phase formation in FE materials, even at the reduced thermal budget of 450 °C.

To analyze the effect of annealing temperature on the formation of the dead layer between the TiN electrode and the HAO FE layer, the interfacial capacitance (C_i) was extracted. To extract the C_i value, a pre-polarization step was first performed by applying a negative pulse at −3.5 MV/cm to fully align the FE dipoles in one direction. Subsequently, polarization switching in the opposite direction was induced by applying positive pulses with increasing field strengths from 2.1 to 3.5 MV/cm, during which the corresponding switching currents (I_{SW}) were measured. According to the polarization reversal model, I_{SW} can be described by the following equations:

$$I_{sw}(t) = I_{sw}^{0} e^{(t-t_0)/R_L C_i} (t_0 < t < t_{sw}) \quad (1)$$

$$I_{sw}^{0}(t) = (E_a - E_C) \cdot \frac{t_f}{R_L} \quad (2)$$

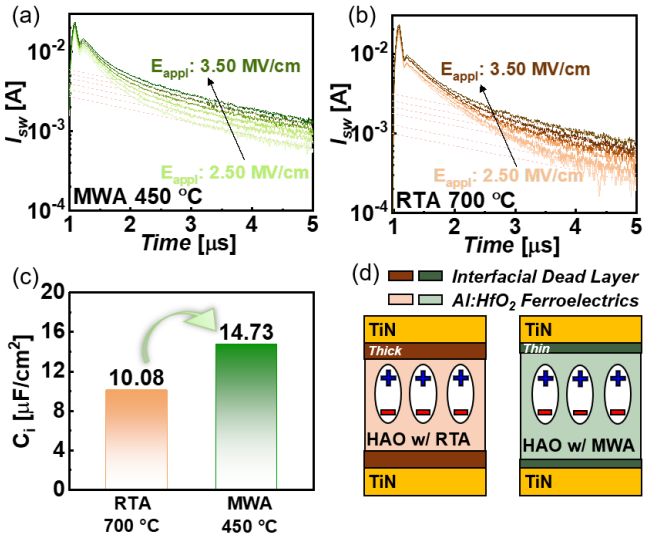

Fig. 3. Transient switching current–time curves of capacitors with (a) MWA and (b) RTA. (c) Comparative analysis of the extracted interfacial dead layer C_i values of capacitors processed via MWA and RTA techniques. (d) Schematic illustrating the configuration of devices subjected to MWA and RTA treatments.

where I_{SW} denotes the switching current at the onset of switching (t_0), R_L represents the total internal resistance, E_a is the applied electric field, E_C is the coercive field, and t_f is the thickness of the FE layer. As shown in Fig. 3(a) and (b), the I_{SW} transient initially exhibits a sharp rise followed by exponential decay, which corresponds to the charging and discharging dynamics of the device. After the switching onset ($t = t_0$), a linear regime in the I_{SW} signal appears due to the actual polarization switching process. By fitting this linear portion with (1) and (2), we were able to extract values for I_{SW}, R_L, and C_i.

An increase in C_i indicates a reduction in the effective thickness of the non-FE layer, implying suppressed formation of the interfacial dead layer [31]. As depicted in Fig. 3(c), the C_i value obtained from the MWA sample is higher than that from the RTA sample, suggesting that the interfacial dead layer was effectively suppressed in the MWA sample. This is attributed to the reduced thermal budget of the MWA process, which inhibits the oxidation of the metal electrode and prevents dead layer formation between the TiN and the HAO film, as illustrated in Fig. 3(d) [28], [29], [32].

Furthermore, the endurance and retention characteristics were carried out to assess the effect of interface quality on the reliability of the HAO thin film. Fig. 4(a) and (b) demonstrates the endurance properties of MWA and RTA annealed capacitors for pulse cycling with an amplitude ranging from 3.0 to 4.5 V and a width of 10 μs. The $2P_r$ values rose owing to the wake-up effect and then gradually decreased. The findings indicate that the devices with MWA exhibit better endurance properties. Fig. 4(c) illustrates the pulse sequence used for the retention measurements. The same-state (SS), new SS (NSS), and opposite-state (OS) retention measurements are widely adopted methodologies for evaluating the retention characteristics of MFM capacitors under various memory operation scenarios in FE random access memory devices [32], [33]. The SS condition is used to assess self-retention behavior, while the

Authorized licensed use limited to: Korea Advanced Inst of Science & Tech - KAIST. Downloaded on December 01,2025 at 09:32:13 UTC from IEEE Xplore. Restrictions apply.

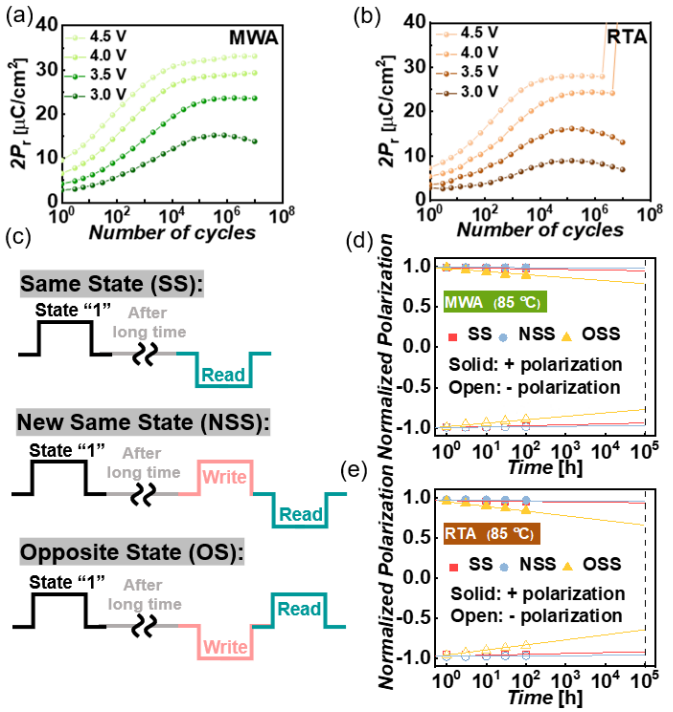

Fig. 4. Endurance characteristics of (a) MWA and (b) RTA capacitors with respect to various pulse voltages. (c) Pulse profiles of retention measurement. Obtained retention properties of devices fabricated with (d) MWA and (e) RTA techniques.

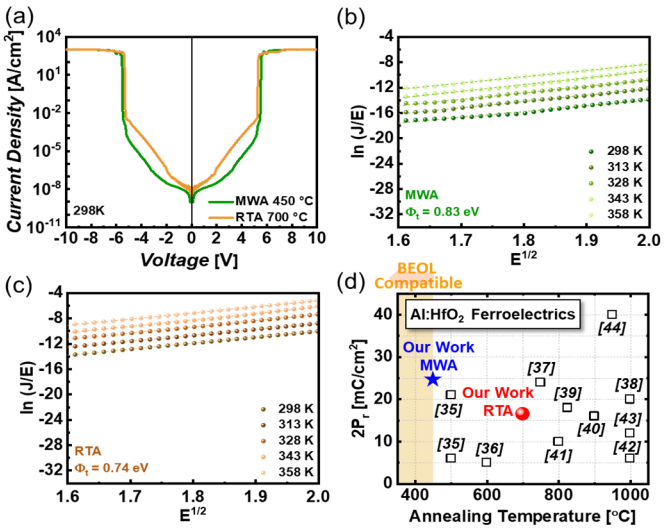

Fig. 5. (a) Comparison of leakage current of capacitors formed by MWA and RTA processes. Poole–Frenkel plots for the devices with (b) MWA and (c) RTA treatments. (d) Benchmark comparison of $2P_r$ values achieved in HAO FE films.

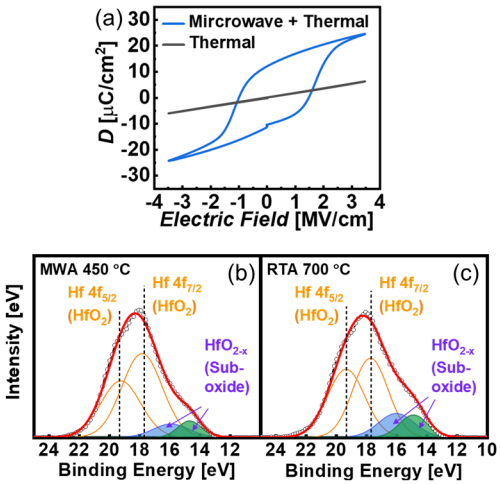

Fig. 6. (a) Dielectric displacement responses of HAO films annealed at 450 °C under combined microwave and thermal energy versus those annealed with thermal energy only, as a function of electric field. XPS depth profile analysis of HAO films annealed using (b) MWA system at 450 °C and (c) RTA system at 700 °C.

NSS condition reflects realistic usage scenarios by applying mixed logic states. The OS condition evaluates the retention stability after switching to the opposite logic state, thereby highlighting the effects of the built-in field and polarization reversal fatigue.

Fig. 4(d) and (e) shows the retention characteristics of the MWA and RTA samples, respectively, measured at 85 °C. Both samples exhibit excellent retention under SS and NSS conditions; however, noticeable degradation is observed under the OS condition. In particular, the RTA sample shows more severe degradation, which can be attributed to the increased susceptibility of the HAO film to thermal depolarization caused by the formation of interfacial dead layers and a higher concentration of oxygen vacancies [32], [33].

Fig. 5(a) depicts the comparison of the leakage current of capacitors formed by MWA and RTA processes. The MWA capacitor demonstrated a lower leakage current density at 1 V, with a reduction of 68%, from 3.89×10^{-8} A/cm^2 for the RTA sample to 1.26×10^{-8} A/cm^2 for the MWA sample. To demonstrate that the low-temperature annealing process of the MWA system is the primary factor contributing to the improvement in the leakage current characteristics of the MFM capacitor, we examined the traps present within the HAO material. Fig. 5(b) and (c) demonstrates a clear linear correlation between $\ln(J/E)$ and $E^{1/2}$, signifying that Poole–Frenkel (P–F) emission predominates as the conduction mechanism within this region. The RTA sample generated a relatively shallow trap with an energy level of 0.74 eV, while the MWA sample exhibited a deeper trap level of 0.83 eV. This suggests that the MWA annealing system suppresses the formation of shallow traps in the HAO material compared to the typical RTA system, which could lead to improved leakage current characteristics and enhanced reliability [34]. The $2P_r$ values of the HAO thin films annealed at various temperatures are benchmarked in Fig. 5(d), emphasizing our record achievement at low annealing temperatures and enhanced $2P_r$ value [35], [36], [37], [38], [39], [40], [41], [42], [43], [44]. This study is significant as it successfully achieves superior polarization switching in HAO FE material under low thermal budget conditions (450 °C), by utilizing the MWA system [45], [46], [47].

This study experimentally demonstrated that low-temperature crystallization of HAO thin films can be achieved via MWA. However, the individual contributions of microwave energy and thermal energy to the crystallization process have not been quantitatively evaluated, presenting a

Authorized licensed use limited to: Korea Advanced Inst of Science & Tech - KAIST. Downloaded on December 01,2025 at 09:32:13 UTC from IEEE Xplore. Restrictions apply.

limitation of this work. To explore this aspect, we attempted to crystallize HAO thin films using only thermal energy at 450 °C, without microwave irradiation, as shown in Fig. 2. No crystallization was observed under these conditions, suggesting the presence of a synergistic effect between thermal and microwave energy inputs in promoting FE phase formation [Fig. 6(a)]. Further studies, including modeling-based approaches, are required to quantitatively compare these two effects and to elucidate the mechanism of their synergy in the crystallization of hafnia-based FE materials.

Fig. 6(b) and (c) shows the XPS depth profiles of HAO films annealed using MWA at 450 °C and RTA at 700 °C for 10 s, respectively. Based on previous reports indicating that thermal treatment of FE capacitors promotes dead layer formation at the bottom interface between the bottom metal and the hafnia FE layer [32], the analysis focused on the bottom interface region. The MWA-treated sample exhibited approximately 13% HfO_{2-x} suboxide content, whereas the RTA-treated sample showed a higher suboxide concentration of around 22%. These results suggest that low-temperature annealing enabled by the MWA system effectively suppresses undesirable interfacial reactions between the FE film and the TiN electrode.

IV. Conclusion

In this research, we address the critical challenge associated with the high-temperature annealing of HAO FE materials by introducing the MWA system. This innovative technique synergistically employs heat and microwaves to efficiently induce phase transformation for FE materials. Consequently, HAO is transformed into a high-quality o-phase, characterized by a notable $2P_r$ of 24.63 μC/cm^2, at a significantly reduced temperature of 450 °C. Moreover, the MWA-based low-temperature process improves the interface quality between the metal and HAO, surpassing the outcomes with conventional RTA at 700 °C. These advancements not only enhance reliability but also reduce leakage current in HAO capacitors.

References

[1] J. Hwang, C. Kim, J. Ahn, and S. Jeon, "Enhanced performance of hafnia self-rectifying ferroelectric tunnel junctions at cryogenic temperatures," *Nano Converg.*, vol. 11, no. 1, pp. 1–9, 2024, doi: 10.1186/s40580-024-00461-2.

[2] S. Nam and M. Kim, "Advances in materials and technologies for digital light processing 3D printing," *Nano Converg.*, vol. 11, no. 1, p. 45, Nov. 2024, doi: 10.1186/s40580-024-00452-3.

[3] J. Lee et al., "Role of oxygen vacancies in ferroelectric or resistive switching hafnium oxide," *Nano Converg.*, vol. 10, no. 1, p. 55, Dec. 2023, doi: 10.1186/s40580-023-00403-4.

[4] S. Lee et al., "Design guidelines of Hafnia ferroelectrics and gate-stack for multilevel-cell FeFET," *IEEE Trans. Electron Devices*, vol. 71, no. 3, pp. 1865–1871, Mar. 2024, doi: 10.1109/TED.2024.3355873.

[5] H. Shin et al., "A method of controlling the imprint effect in Hafnia ferroelectric device," *Appl. Phys. Lett.*, vol. 122, no. 2, Jan. 2023, Art. no. 022901, doi: 10.1063/5.0123312.

[6] G. Kim et al., "Design guidelines of thermally stable Hafnia ferroelectrics for the fabrication of 3D memory devices," in *IEDM Tech. Dig.*, Dec. 2022, pp. 5.4.1–5.4.4, doi: 10.1109/IEDM45625.2022.10019458.

[7] U. Schroeder, M. H. Park, T. Mikolajick, and C. S. Hwang, "The fundamentals and applications of ferroelectric HfO_2," *Nature Rev. Mater.*, vol. 7, no. 8, pp. 653–669, Mar. 2022, doi: 10.1038/s41578-022-00431-2.

[8] S. Song et al., "Highly stable artificial synapses based on ferroelectric tunnel junctions for neuromorphic computing applications," *Adv. Mater. Technol.*, vol. 7, no. 7, Jul. 2022, Art. no. 2101323, doi: 10.1002/admt.202101323.

[9] M. Hellenbrand and J. MacManus-Driscoll, "Multi-level resistive switching in hafnium-oxide-based devices for neuromorphic computing," *Nano Converg.*, vol. 10, no. 1, p. 44, Sep. 2023, doi: 10.1186/s40580-023-00392-4.

[10] H. Joh, S. Nam, M. Jung, H. Shin, S. H. Cho, and S. Jeon, "Ferroelectric Hafnia-based M3D FeTFTs annealed at extremely low temperatures and TCAM cells for computing-in-memory applications," *ACS Appl. Mater. Interfaces*, vol. 15, no. 44, pp. 51339–51349, Nov. 2023, doi: 10.1021/acsami.3c10597.

[11] C.-Y. Teng et al., "Optimizing the ferroelectric properties of $Hf_{1-x}Zr_xO_2$ films via crystal orientation," *ACS Appl. Electron. Mater.*, vol. 5, no. 2, pp. 1114–1122, Feb. 2023, doi: 10.1021/acsaelm.2c01582.

[12] D. Wang et al., "Enhanced ferroelectric polarization with less wake-up effect and improved endurance of $Hf_{0.5}Zr_{0.5}O_2$ thin films by implementing W electrode," *J. Mater. Sci. Technol.*, vol. 104, pp. 1–7, Mar. 2022, doi: 10.1016/j.jmst.2021.07.016.

[13] B. Buyantogtokh, V. Gaddam, and S. Jeon, "Effect of high pressure anneal on switching dynamics of ferroelectric hafnium zirconium oxide capacitors," *J. Appl. Phys.*, vol. 129, no. 24, Jun. 2021, Art. no. 244106, doi: 10.1063/5.0050535.

[14] J. Hwang et al., "Relatively low-k ferroelectric nonvolatile memory using fast ramping fast cooling annealing process," *IEEE Trans. Electron Devices*, vol. 69, no. 6, pp. 3439–3445, Jun. 2022, doi: 10.1109/TED.2022.3165167.

[15] G. Kim et al., "Novel strategies for low-voltage NAND flash memory with negative capacitance effect," *Jpn. J. Appl. Phys.*, vol. 63, no. 5, May 2024, Art. no. 05SP06, doi: 10.35848/1347-4065/ad3f23.

[16] L. Yin et al., "Improvement of ferroelectricity and endurance in Sr doped $Hf_{0.5}Zr_{0.5}O_2$ films," *J. Alloys Compounds*, vol. 914, Sep. 2022, Art. no. 165301, doi: 10.1016/j.jallcom.2022.165301.

[17] Y. Yun et al., "Intrinsic ferroelectricity in Y-doped HfO_2 thin films," *Nature Mater.*, vol. 21, no. 8, pp. 903–909, Aug. 2022, doi: 10.1038/s41563-022-01282-6.

[18] S. Belahcen, T. Francois, L. Grenouillet, A. Bsiesy, J. Coignus, and M. Bonvalot, "TiN/gd:HfO_2/TiN capacitors grown by PEALD showing high endurance ferroelectric switching," *Appl. Phys. Lett.*, vol. 117, no. 25, Dec. 2020, Art. no. 252903, doi: 10.1063/5.0035706.

[19] J. Zhou et al., "Al-doped and deposition temperature-engineered HfO_2 near morphotropic phase boundary with record dielectric permittivity (∼68)," in *IEDM Tech. Dig.*, Dec. 2021, pp. 13.4.1–13.4.4, doi: 10.1109/IEDM19574.2021.9720632.

[20] Y. Choi, J. Shin, S. Moon, J. Min, C. Han, and C. Shin, "Experimental study of endurance characteristics of Al-doped HfO_2 ferroelectric capacitor," *Nanotechnology*, vol. 34, no. 18, Feb. 2023, Art. no. 185203, doi: 10.1088/1361-6528/acb7fc.

[21] T. Francois et al., "Demonstration of BEOL-compatible ferroelectric $Hf_{0.5}Zr_{0.5}O_2$ scaled FeRAM co-integrated with 130nm CMOS for embedded NVM applications," in *IEDM Tech. Dig.*, Dec. 2019, pp. 15.7.1–15.7.4, doi: 10.1109/IEDM19573.2019.8993485.

[22] L. Grenouillet et al., "Nanosecond laser anneal (NLA) for Si-implanted HfO_2 ferroelectric memories integrated in back-end of line (BEOL)," in *Proc. IEEE Symp. VLSI Technol.*, Jun. 2020, pp. 1–2, doi: 10.1109/VLSITechnology18217.2020.9265061.

[23] S. J. Kim et al., "Effect of film thickness on the ferroelectric and dielectric properties of low-temperature (400 °C) $Hf_{0.5}Zr_{0.5}O_2$ films," *Appl. Phys. Lett.*, vol. 112, no. 17, Apr. 2018, Art. no. 172902, doi: 10.1063/1.5026715.

[24] T. Onaya et al., "Ferroelectricity of $Hf_xZr_{1-x}O_2$ thin films fabricated using TiN stressor and ZrO_2 nucleation techniques," *ECS Trans.*, vol. 86, no. 6, pp. 31–38, Jul. 2018, doi: 10.1149/08606.0031ecst.

[25] S. J. Kim et al., "Large ferroelectric polarization of TiN/$Hf_{0.5}Zr_{0.5}O_2$/TiN capacitors due to stress-induced crystallization at low thermal budget," *Appl. Phys. Lett.*, vol. 111, no. 24, Dec. 2017, Art. no. 242901, doi: 10.1063/1.4995619.

[26] S. J. Kim et al., "Effect of hydrogen derived from oxygen source on low-temperature ferroelectric TiN/$Hf_{0.5}Zr_{0.5}O_2$/TiN capacitors," *Appl. Phys. Lett.*, vol. 115, no. 18, Oct. 2019, Art. no. 182901, doi: 10.1063/1.5126144.

[27] T. Jung, J. H. Han, S. Nam, and S. Jeon, "Enhancement of electrical properties of a-IGZO thin film transistor by low temperature (150 °C) microwave annealing for flexible electronics," *J. Vac. Sci. Technol. B*, vol. 41, no. 3, Apr. 2023, Art. no. 032201, doi: 10.1116/6.0002343.

Authorized licensed use limited to: Korea Advanced Inst of Science & Tech - KAIST. Downloaded on December 01,2025 at 09:32:13 UTC from IEEE Xplore. Restrictions apply.

[28] M. Jung et al., "Flexible artificial mechanoreceptor based on microwave annealed morphotropic phase boundary of $Hf_xZr_{1-x}O_2$ thin film," *Adv. Electron. Mater.*, vol. 10, no. 2, Feb. 2024, Art. no. 2300594, doi: 10.1002/aelm.202300594.

[29] H. Joh, M. Jung, J. Hwang, Y. Goh, T. Jung, and S. Jeon, "Flexible ferroelectric Hafnia-based synaptic transistor by focused-microwave annealing," *ACS Appl. Mater. Interfaces*, vol. 14, no. 1, pp. 1326–1333, Jan. 2022, doi: 10.1021/acsami.1c16873.

[30] M. H. Park et al., "Effect of Zr content on the wake-up effect in $Hf_{1-x}Zr_xO_2$ films," *ACS Appl. Mater. Interfaces*, vol. 8, no. 24, pp. 15466–15475, Jun. 2016, doi: 10.1021/acsami.6b03586.

[31] D. Das, B. Buyantogtokh, V. Gaddam, and S. Jeon, "Influence of high-pressure annealing conditions on ferroelectric and interfacial properties of Zr-rich $Hf_xZr_{1-x}O_2$ capacitors," *IEEE Trans. Electron Devices*, vol. 68, no. 4, pp. 1996–2002, Apr. 2021, doi: 10.1109/TED.2021.3061963.

[32] Y. Goh, S. H. Cho, S.-H.-K. Park, and S. Jeon, "Oxygen vacancy control as a strategy to achieve highly reliable Hafnia ferroelectrics using oxide electrode," *Nanoscale*, vol. 12, no. 16, pp. 9024–9031, 2020, doi: 10.1039/d0nr00933d.

[33] F. Mehmood et al., "Bulk depolarization fields as a major contributor to the ferroelectric reliability performance in lanthanum doped $Hf_{0.5}Zr_{0.5}O_2$ capacitors," *Adv. Mater. Interfaces*, vol. 6, no. 21, Nov. 2019, Art. no. 1901180, doi: 10.1002/admi.201901180.

[34] F.-C. Chiu, "A review on conduction mechanisms in dielectric films," *Adv. Mater. Sci. Eng.*, vol. 2014, pp. 1–18, Feb. 2014, doi: 10.1155/2014/578168.

[35] J. Zhou et al., "Demonstration of ferroelectricity in Al-doped HfO_2 with a low thermal budget of 500 °C," *IEEE Electron Device Lett.*, vol. 41, no. 7, pp. 1130–1133, Jul. 2020, doi: 10.1109/LED.2020.2998355.

[36] K.-Y. Chen, K.-L. Chu, P.-H. Chen, and Y.-H. Wu, "Ferroelectricity of low thermal-budget $HfAlO_x$ for devices with metal–ferroelectric–insulator–semiconductor structure," *RSC Adv.*, vol. 6, no. 78, pp. 74445–74452, Aug. 2016, doi: 10.1039/c6ra09987d.

[37] K. Florent et al., "First demonstration of vertically stacked ferroelectric Al doped HfO_2 devices for NAND applications," in *Proc. Symp. VLSI Technol.*, Jun. 2017, pp. T158–T159, doi: 10.23919/VLSIT.2017.7998162.

[38] S. Mueller et al., "Incipient ferroelectricity in Al-doped HfO_2 thin films," *Adv. Funct. Mater.*, vol. 22, no. 11, pp. 2412–2417, Jun. 2012, doi: 10.1002/adfm.201103119.

[39] A. Nourbakhsh, A. Zubair, S. Joglekar, M. Dresselhaus, and T. Palacios, "Subthreshold swing improvement in MoS_2 transistors by the negative-capacitance effect in a ferroelectric Al-doped-HfO_2/HfO_2 gate dielectric stack," *Nanoscale*, vol. 9, no. 18, pp. 6122–6127, May 2017, doi: 10.1039/c7nr00088j.

[40] C.-C. Fan, C.-H. Cheng, Y.-R. Chen, C. Liu, and C.-Y. Chang, "Energy-efficient $HfAlO_x$ NCFET: Using gate strain and defect passivation to realize nearly hysteresis-free sub-25 mV/dec switch with ultralow leakage," in *IEDM Tech. Dig.*, Dec. 2017, pp. 23.2.1–23.2.4, doi: 10.1109/IEDM.2017.8268444.

[41] T. Srimani et al., "Negative capacitance carbon nanotube FETs," *IEEE Electron Device Lett.*, vol. 39, no. 2, pp. 304–307, Feb. 2018, doi: 10.1109/LED.2017.2781901.

[42] W. C. Yap, H. Jiang, J. Liu, Q. Xia, and W. Zhu, "Ferroelectric transistors with monolayer molybdenum disulfide and ultra-thin aluminum-doped hafnium oxide," *Appl. Phys. Lett.*, vol. 111, no. 1, Jul. 2017, Art. no. 013103, doi: 10.1063/1.4991877.

[43] J. L. Eschle, "Annealing study of ALD deposited ferroelectric aluminum-doped hafnium oxide," *J. Microelectron. Eng. Conf.*, vol. 24, no. 1, p. 19, Apr. 2018. [Online]. Available: https://repository.rit.edu/ritamec/vol24/iss1/19

[44] H. Ryu, K. Xu, J. Kim, S. Kang, J. Guo, and W. Zhu, "Exploring new metal electrodes for ferroelectric aluminum-doped hafnium oxide," *IEEE Trans. Electron Devices*, vol. 66, no. 5, pp. 2359–2364, May 2019, doi: 10.1109/TED.2019.2907070.

[45] B. Cui et al., "Back-end-of-line compatible HfO_2/ZrO_2 superlattice ferroelectric capacitor with high endurance and remnant polarization," *IEEE Electron Device Lett.*, vol. 44, no. 6, pp. 1011–1014, Jun. 2023, doi: 10.1109/LED.2023.3265516.

[46] X. Wang, X. Shi, X. Xiong, R. Huang, and Y. Wu, "BEOL compatible high-performance monolayer WSe_2 pFETs with record Gm=190 μS/μm and Ion=350 μA/μm by direct-growth on SiO_2 substrate at reduced temperatures," in *IEDM Tech. Dig.*, Dec. 2023, pp. 1–4, doi: 10.1109/IEDM45741.2023.10413833.

[47] M. H. Ali et al., "Enhanced polarization, endurance, and long retention in low temperature processed W/$Hf_{0.5}Zr_{0.5}O_2$/W ferroelectric capacitor for back-end-of-line integration," in *Proc. 8th IEEE Electron Devices Technol. Manuf. Conf. (EDTM)*, Mar. 2024, pp. 1–3, doi: 10.1109/EDTM58488.2024.10511921.

Authorized licensed use limited to: Korea Advanced Inst of Science & Tech - KAIST. Downloaded on December 01,2025 at 09:32:13 UTC from IEEE Xplore. Restrictions apply.